

Interaction of photons with silver and indium nuclei at energies up to 20 MeV*

J. H. Khushvaktov^{1,2†} M. A. Demichev¹ D. L. Demin¹ S. A. Evseev¹ M. I. Gostkin¹ V. V. Kobets¹ F. A. Rasulova^{1,2} S. V. Rozov¹ E. T. Ruziev² A. A. Solnyshkin¹ T. N. Tran^{1,3} E. A. Yakushev¹ B. S. Yuldashev^{1,2}

¹Joint Institute for Nuclear Research (JINR), Dubna, Russia

²Institute of Nuclear Physics of the Academy of Sciences of the Republic of Uzbekistan (INP ASRU), Tashkent, Uzbekistan

³Institute of Physics of the Vietnam Academy of Science and Technology (IP VAST), Hanoi, Vietnam

Abstract: The yields of photonuclear reactions in the ^{107}Ag , ^{113}In , and ^{115}In nuclei were measured. Monte Carlo simulations were performed using the Geant4 code, and the results were compared with the experimental values. The isomeric ratios of the yields in the reactions $^{107}\text{Ag}(\gamma, n)^{106m,g}\text{Ag}$ and $^{113}\text{In}(\gamma, n)^{112m,g}\text{In}$ were determined, and the cross sections for the reactions $^{107}\text{Ag}(\gamma, n)^{106g}\text{Ag}$ and $^{107}\text{Ag}(\gamma, 2n)^{105}\text{Ag}$ at an energy of 20 MeV were calculated based on the experimental data.

Keywords: $^{107}\text{Ag}(\gamma, n)^{106m,g}\text{Ag}$ and $^{113}\text{In}(\gamma, n)^{112m,g}\text{In}$ reactions, cross section, yield, isomeric ratio, simulation, Geant4, TALYS

DOI: 10.1088/1674-1137/ad1028

I. INTRODUCTION

The study of the isomeric states of atomic nuclei provides information on the nature of the excited states of atomic nuclei [1–6]. The phenomenon of atomic nucleus isomerism is associated with a significant difference in the spin or deformation of the isomeric state relative to the ground state of an atomic nucleus. The probability of isomer population resulting from photonuclear reactions depends on the reaction energy, orbital momentum of emitted particles, momentum and parity of the final state, and probabilities of cascade transitions from higher-lying states [7]. In this study, in addition to the isomeric ratios, the yields and cross sections of photonuclear reactions in silver and indium samples were investigated.

Natural silver consists of two stable isotopes, with isotope abundances of 51.84% (^{107}Ag) and 48.16% (^{109}Ag). The ^{107}Ag and ^{109}Ag nuclei have $Z = 47$ protons. From the perspective of the shell model, this is a three-proton-hole state with respect to the magic number $Z = 50$. The number of neutrons in these is $N = 60$ and 62 , respectively. The ground states of ^{107}Ag ($J^\pi = 1/2^-$) and ^{109}Ag ($J^\pi = 1/2^-$) are formed as a result of an interaction between two fairly complex proton and neutron configurations [8]. Natural indium also consists of two isotopes, the stable ^{113}In (4.29%) and beta radioactive ^{115}In (95.71%; half-life 4.41×10^{14} years). The number of protons in the odd-even

nuclei of ^{113}In and ^{115}In is close to the magic number $Z = 50$, and the number of neutrons is $N = 64$ and 66 , respectively. The spin-parity of the ground state of ^{113}In and ^{115}In is determined by the $1g_{9/2}$ subshell, which contains nine protons [9].

II. EXPERIMENTAL DESIGN AND DATA ANALYSIS

The experiments were performed at the LINAC-200 electron accelerator [10]. A tungsten converter with a size of $4.5 \times 4.5 \times 0.5$ cm was irradiated with 20-MeV electron beams. Samples of silver and indium with dimensions of $0.7 \times 0.6 \times 0.1$ cm and $1.0 \times 0.7 \times 0.1$ cm, respectively, were placed behind the tungsten converter. The $^{\text{nat}}\text{Ag}$ and $^{\text{nat}}\text{In}$ samples were irradiated with a bremsstrahlung flux generated in the tungsten converter during electron beam irradiation with an irradiation time of 40 min, pulse current of 20 mA, pulse frequency of 10 Hz, and pulse duration of 2 μs . The pulse current was measured with an inductive current sensor based on a Rogowski coil. After irradiation, the silver and indium samples were transferred to the test room, and their gamma spectra were measured using a HPGe detector. Eight gamma spectra were measured for each sample with different measurement times. The times from the

Received 22 August 2023; Accepted 27 November 2023; Published online 28 November 2023

* The authors express their gratitude to the team of the LINAC-200 electron accelerator and the management of the Joint Institute for Nuclear Research for their support in conducting the experiments.

† E-mail: khushvaktov@jinr.ru

©2024 Chinese Physical Society and the Institute of High Energy Physics of the Chinese Academy of Sciences and the Institute of Modern Physics of the Chinese Academy of Sciences and IOP Publishing Ltd

end of irradiation to the beginning of the measurement of the first spectrum of the ^{nat}Ag and ^{nat}In samples were 27 and 36 min, respectively. The gamma spectra obtained were processed using the Deimos32 program [11]. The areas of the identified peaks were determined with the background from the Compton scattering of photons subtracted. The absolute efficiency of the HPGe detector was measured using standard gamma-ray sources at the same distances from the detector at which the silver and indium samples were examined. The set of gamma-ray sources consisted of ^{54}Mn , ^{57}Co , ^{60}Co , ^{88}Y , ^{109}Cd , ^{113}Sn , ^{133}Ba , ^{139}Ce , ^{152}Eu , ^{228}Th , and ^{241}Am . The yields of photo-nuclear reactions in the samples were determined using the following formula [12]:

$$Y_{\text{exp}} = \frac{S_p \cdot C_{\text{abs}} t_{\text{real}}}{\varepsilon_p \cdot I_\gamma} \frac{1}{t_{\text{live}}} \frac{1}{N} \frac{1}{N_{e^-}} \frac{e^{-\lambda t_{\text{cool}}}}{1 - e^{-\lambda t_{\text{real}}}} \frac{\lambda \cdot t_{\text{irr}}}{1 - e^{-\lambda t_{\text{irr}}}}, \quad (1)$$

where S_p is the full-energy peak area, ε_p is the full-energy peak detector efficiency, C_{abs} is the self-absorption correction coefficient, I_γ is the gamma emission probability, t_{real} and t_{live} are the real and live times of the measurement, respectively, N is the number of atoms in a sample, N_{e^-} is the integral number of electrons incident on the tungsten converter, λ is the decay constant, t_{cool} is the cooling time, and t_{irr} is the irradiation time.

The parameter values of the nuclear reactions investigated in this study according to data from [13] and the yields of the measured nuclear reactions are given in Table 1, where E_{th} represents the reaction thresholds, J , π , and $T_{1/2}$ are the spin, parity, and half-life of the nuclear reaction products, respectively, E_γ represents the energies of gamma rays emitted by the reaction products, and Y_{exp} denotes the yields of the reactions. The values of the reaction thresholds E_{th} were obtained from the TALYS-1.96 program [14]. The reaction yields for all the identified gamma rays of radionuclides given in Table 1 were calculated using formula (1). Subsequently, when a radionuclide was identified with more than one gamma line, their reaction yield values were averaged, as given in Table 2.

III. MONTE CARLO SIMULATION

Currently, Geant4 [15], FLUKA [16], and MCNP6 [17] are the most common Monte Carlo radiation transport codes for photonuclear reaction studies. In this study, we performed simulations with the Geant4 code. To simulate photonuclear interactions in Geant4, the G4PhotoNuclearProcess class [18] was used. Owing to the difficulty in using a sufficient number of electrons to determine the number of photonuclear reactions with a small uncertainty, we only obtained the fluences of electrons, bremsstrahlung, and neutrons in Geant4 calculations. Furthermore, the yields of the photonuclear reaction and the

reaction of neutron capture by the nucleus were determined using formula (2). The reaction cross sections were calculated using the TALYS-1.96 program.

$$Y_{\text{calc}} = \int_{E_{\text{thr}}}^{E_{\text{max}}} f(E) \sigma(E) dE, \quad (2)$$

where $f(E)$ is the bremsstrahlung fluence (in the case of the neutron capture reaction, the neutron fluence), and $\sigma(E)$ is the reaction cross section.

IV. RESULTS AND DISCUSSION

Using the results of processing the measured gamma spectra, we identified photoneutron reactions with the release of up to two neutrons from nuclei, the inelastic scattering of photons in nuclei, and the capture reaction of secondary neutrons by the nucleus. Table 2 shows the yields of the above reactions in the ^{107}Ag , ^{113}In , and ^{115}In nuclei per electron incident on the tungsten converter with an energy of 20 MeV and their comparison with the simulation results.

According to the Nilsson model, the ground state in ^{106}Ag (1^+) can be described as the result of the addition of the proton state $1/2^-$ to the deformed neutron state $1/2^-$ arising from the splitting of the $1h11/2$ shell level. The $J^\pi=6^+$ state can be obtained by adding the proton level $7/2^+$ to the neutron level $5/2^+$ formed upon the splitting of the $1g7/2$ level in the deformed potential [8]. For the isomeric pair of odd-odd ^{112}In nuclei, the spin-parity of the metastable state is $J^\pi=4^+$, and for the ground state, it is $J^\pi=1^+$. One unpaired proton located on the $1g9/2$ subshell and a neutron, for example, on the $3s1/2$ subshell, form the $J^\pi=4^+$ isomeric state. To form the ground state, the neutron must be on a subshell with a large spin ($7/2$) to form the $J^\pi=1^+$ state together with the proton shell $9/2^+$ [9].

A. Isomeric yield ratio

According to the experimental data obtained, we determined the isomeric ratios of $^{112m}\text{In}/^{112g}\text{In}$ and $^{106m}\text{Ag}/^{106g}\text{Ag}$. To determine the isomeric ratios of the yield in the photoneutron reaction $^{113}\text{In}(\gamma, n)^{112m,g}\text{In}$, the following formula (3) was used:

$$\frac{Y_m}{Y_g} = \left[\frac{\lambda_g (1 - e^{-\lambda_m t_{\text{irr}}}) e^{-\lambda_m t_{\text{cool}}} (1 - e^{-\lambda_m t_{\text{real}}})}{\lambda_m (1 - e^{-\lambda_g t_{\text{irr}}}) e^{-\lambda_g t_{\text{cool}}} (1 - e^{-\lambda_g t_{\text{real}}})} \times \left(\frac{S_{p,g} I_{\gamma,m} \varepsilon_{p,m} C_{\text{abs},m}}{S_{p,m} I_{\gamma,g} \varepsilon_{p,g} C_{\text{abs},g}} - p \frac{\lambda_g}{\lambda_g - \lambda_m} \right) + p \frac{\lambda_m}{\lambda_g - \lambda_m} \right]^{-1}, \quad (3)$$

where p is the branching ratio.

The half-life of the ^{112m}In (4^+) isomeric state was

Table 1. Spectroscopic data [13] on the nuclei products and experimental yields of measured nuclear reactions.

Nuclear reaction	E_{th} /MeV	J^π of nucleus-product	$T_{1/2}$	E_γ /keV	I_γ /%	Y_{exp} (atom ⁻¹ · electron ⁻¹)
$^{107}\text{Ag}(\gamma, n)^{106m}\text{Ag}$	9.55	6^+	8.28 (2) d	511.842 (28)	88 (3)	5.04(31)E-29
				1045.83 (8)	29.6 (10)	4.79(26)E-29
				717.24 (6)	28.9 (8)	5.00(26)E-29
				450.97 (3)	28.2 (7)	4.95(26)E-29
				616.174 (24)	21.6 (6)	4.77(25)E-29
				748.44 (7)	20.6 (6)	4.63(25)E-29
				1527.65 (19)	16.3 (13)	5.15(34)E-29
				824.79 (15)	15.3 (4)	4.89(26)E-29
				406.17 (3)	13.4 (4)	5.15(28)E-29
				429.64 (5)	13.2 (4)	4.93(26)E-29
				804.34 (13)	12.4 (5)	4.82(27)E-29
				1128.00 (6)	11.8 (5)	5.25(30)E-29
				1199.39 (10)	11.2 (5)	5.20(30)E-29
$^{107}\text{Ag}(\gamma, n)^{106g}\text{Ag}$	9.55	1^+	23.96 (4) min	621.94 (3)	0.316 (8)	4.99(28)E-27
				873.48 (4)	0.199 (5)	4.76(29)E-27
				1050.39 (5)	0.167 (5)	4.61(32)E-27
				616.174 (24)	0.142 (5)	4.79(32)E-27
				1128.00 (6)	0.0721 (25)	5.18(40)E-27
				1194.53 (4)	0.0398 (25)	4.39(52)E-27
				1562.24 (5)	0.0172 (5)	4.12(70)E-27
$^{107}\text{Ag}(\gamma, 2n)^{105}\text{Ag}$	17.56	$1/2^-$	41.29 (7) d	344.520 (21)	41 (1)	2.28(13)E-29
				280.41 (6)	30.2 (17)	2.28(14)E-29
				63.98 (3)	10.5 (10)	2.50(20)E-29
$^{113}\text{In}(\gamma, \gamma^+)^{113m}\text{In}$	1.45	$1/2^-$	1.658 (1) h	443.37 (7)	10.5 (5)	1.95(13)E-29
				319.14 (6)	4.35 (21)	2.10(23)E-29
$^{113}\text{In}(\gamma, n)^{112m}\text{In}$	9.55	4^+	20.56 (6) min	391.690 (15)	64.2 (1)	2.56(11)E-28
				156.56 (10)	13.2 (3)	1.30(7)E-27
$^{113}\text{In}(\gamma, n)^{112g}\text{In}$	9.55	1^+	14.97 (10) min	617.516 (11)	4.6 (1)	4.40(47)E-28
				606.88 (15)	1.111 (19)	4.10(45)E-28
$^{113}\text{In}(\gamma, 2n)^{111}\text{In}$	17.23	$9/2^+$	2.8047 (5) d	245.395 (20)	94 (1)	3.19(15)E-29
				171.28 (3)	90 (1)	3.07(15)E-29
				1293.558 (15)	84.4 (17)	1.93(8)E-29
				1097.326 (22)	56.2 (11)	2.01(9)E-29
				416.86 (3)	27.7 (12)	2.01(9)E-29
$^{115}\text{In}(n, \gamma)^{116m}\text{In}$	-	5^+	54.29 (17) min	2112.312 (22)	15.5 (4)	1.97(10)E-29
				818.718 (21)	11.5 (4)	2.04(10)E-29
				1507.67 (4)	10.0 (3)	1.97(10)E-29
$^{115}\text{In}(\gamma, \gamma^+)^{115m}\text{In}$	1.27	$1/2^-$	4.486 (4) h	336.240 (12)	45.83 (10)	6.98(25)E-29
				190.29 (3)	15.56 (15)	1.72(6)E-27
$^{115}\text{In}(\gamma, n)^{114m}\text{In}$	9.28	5^+	49.51 (1) d	558.456 (2)	3.24 (23)	2.02(10)E-27
				725.298 (9)	3.24 (23)	1.95(10)E-27

Table 2. Experimental yields of measured reactions [$\text{atom}^{-1} \cdot \text{electron}^{-1}$].

Reaction	Yield(Exp.)	Calc./Exp.	Reaction	Yield(Exp.)	Calc./Exp.
$^{107}\text{Ag}(\gamma, n)^{106m}\text{Ag}$	4.94(50)E-29	1.05(11)	$^{113}\text{In}(\gamma, n)^{112g}\text{In}$	4.24(53)E-28	1.97(25)
$^{107}\text{Ag}(\gamma, n)^{106g}\text{Ag}$	4.79(50)E-27	0.40(4)	$^{113}\text{In}(\gamma, 2n)^{111}\text{In}$	3.13(34)E-29	1.69(18)
$^{107}\text{Ag}(\gamma, 2n)^{105}\text{Ag}$	2.20(24)E-29	1.68(18)	$^{115}\text{In}(n, \gamma)^{116m}\text{In}$	1.99(20)E-29	0.83(8)
$^{113}\text{In}(\gamma, \gamma')^{113m}\text{In}$	2.56(28)E-28	0.50(5)	$^{115}\text{In}(\gamma, \gamma')^{115m}\text{In}$	6.98(73)E-29	2.51(27)
$^{113}\text{In}(\gamma, n)^{112m}\text{In}$	1.30(15)E-27	1.91(22)	$^{115}\text{In}(\gamma, n)^{114m}\text{In}$	1.84(21)E-27	1.60(18)

20.56 min. Emitting a gamma quantum with an energy of 156 keV, it decayed to the ground state of ^{112g}In (1^+) via an internal transition with a branching intensity of 100%. The gamma quantum yield in the isomeric transition was 13.2%. The ground state of ^{112g}In (1^+) had a half-life of 14.97 min and decayed via EC to ^{112}Cd with a probability of 62% and via β to ^{112}Sn with a probability of 38%. During the decay of ^{112g}In (1^+), the highest gamma quantum yield was 4.6%, and the corresponding energy was 617.5 keV. The isomeric ratio Y_m/Y_g for the yield of the $^{113}\text{In}(\gamma, n)^{112m,g}\text{In}$ reaction was determined from the area of the gamma ray peaks with energies of 156.6 and 617.5 keV. The yield ratio Y_m/Y_g was 3.15(36), which coincides with the literature data [19–21], as shown in Fig. 1 (a). Using the isomeric ratios Y_m/Y_g of ^{112}In nuclei, the yield of the reaction $^{113}\text{In}(g, n)^{112g}\text{In}$ was determined. The yield value of the reaction $^{113}\text{In}(g, n)^{112m}\text{In}$ given in Table 1 was determined using formula (1).

Determining the isomeric ratios for the ^{106}Ag nucleus was simple. Because the half-lives of the isomeric $J^\pi=6^+$ ($T_{1/2} = 8.28$ d) and ground $J^\pi=1^+$ ($T_{1/2} = 23.96$ min) states of the ^{106}Ag nucleus differed, the independent yields Y_m and Y_g were measured. The isomeric ratio for the ^{106}Ag nucleus was 1.03(11)E-2, which also coincides with literature data [22, 23], as shown in Fig. 1 (b). As shown from the available literature data [7, 13, 19–24, 25–27, 28–30], the average value of the isomeric ratios of $^{112m,g}\text{In}$ in the reaction $^{113}\text{In}(\gamma, n)$ increases with an increase in the end-

point bremsstrahlung energies (see Fig. 1 (a)). The average value of the isomeric ratios of $^{106m,g}\text{Ag}$ in the reaction $^{107}\text{Ag}(\gamma, n)$ in the region of end-point bremsstrahlung energies of 14 to 75 MeV also increases (see Fig. 1 (b)).

B. Reaction cross section

In this study, although investigations on photonuclear reactions were performed with bremsstrahlung, it was still possible to determine the cross sections of photonuclear reactions for a specific photon energy by calculating the monochromatic photon spectrum. The reaction cross section can be determined from the reaction yield data by solving formula (2). A method for calculating the quasi-monoenergetic spectrum from the bremsstrahlung spectrum was shown and used in Ref. [31]. This method was also successfully used in Ref. [32]. In this method, to determine reaction cross sections, the effective photon spectrum must be calculated, the shape of which is close to the spectrum of monoenergetic photons. To calculate the monoenergetic spectrum of photons, we used the calculated bremsstrahlung spectra for electrons with energies of 19, 20, and 21 MeV. When calculating the bremsstrahlung spectra with the Geant4 code, we used the statistics of two billion electrons. The bremsstrahlung spectra of the tungsten converter for electrons with energies of 19, 20 and 21 MeV and the calculated quasi-monoenergetic spectrum of photons with an energy of 20 MeV are shown in Figs. 2 (a) and 2(b), respectively.

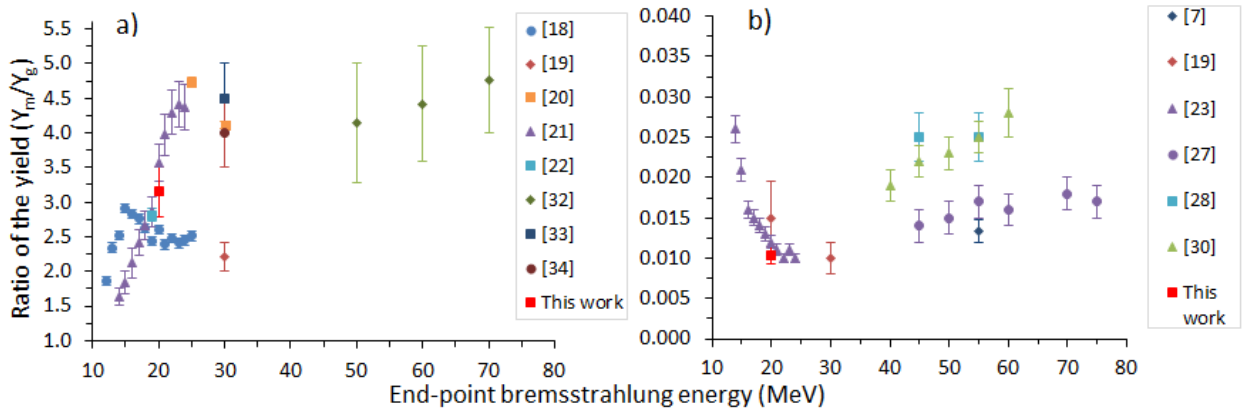


Fig. 1. (color online) Dependence of the isomeric yield ratio in the photoneutron reactions $^{113}\text{In}(\gamma, n)^{112m,g}\text{In}$ (a) and $^{107}\text{Ag}(\gamma, n)^{106m,g}\text{Ag}$ (b) on the end-point bremsstrahlung energy.

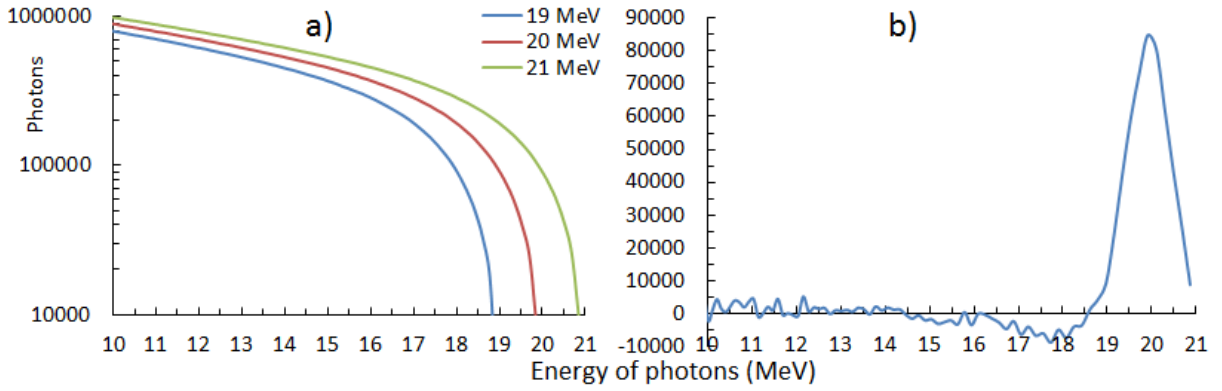


Fig. 2. (color online) Bremsstrahlung spectra of the tungsten converter for electrons with energies of 19, 20, and 21 MeV (a). Quasi-monoenergetic spectrum of 20 MeV photons (b).

To determine the cross section of the reaction, we must determine the value of the yield of the reaction caused by photons with energies of 19 to 21 MeV using the experimental data. To do this, the experimental and calculated values of the yield of the reaction with bremsstrahlung produced by electrons with energies of 19, 20, and 21 MeV were required. We only possessed the experimental value of the reaction yield for electrons with an energy of 20 MeV. Those of the 19 MeV and 21 MeV electrons were corrected from the calculated data by considering the ratios $\frac{Y_{\text{calc}}(19\text{MeV})}{Y_{\text{calc}}(20\text{MeV})} = \frac{Y_{\text{exp}}(19\text{MeV})}{Y_{\text{exp}}(20\text{MeV})}$ and $\frac{Y_{\text{calc}}(21\text{MeV})}{Y_{\text{calc}}(20\text{MeV})} = \frac{Y_{\text{exp}}(21\text{MeV})}{Y_{\text{exp}}(20\text{MeV})}$ to be correct. The cross sections for the photoneutron reactions $^{107}\text{Ag}(\gamma, n)^{106g}\text{Ag}$ and $^{107}\text{Ag}(\gamma, 2n)^{105}\text{Ag}$ at an energy of 20 MeV determined using the above method were 19.0 ± 5.7 mb and 29.4 ± 10.0 mb, respectively, which coincide with literature data [33–35] measured with mono-energetic photons, as shown in Figs. 3 (a) and 3 (b). The values of the flux-weighted average cross-sections at bremsstrahlung endpoint energies from literature data [36] are also shown in Figs. 3 (a) and 3 (b). A region of giant dipole resonance

(9–21 MeV), in which only one nucleon is excited when a γ -quantum is absorbed by the nucleus, can be observed in Fig. 3 (a). Above this region, the quasideuteron mechanism of photoabsorption began to dominate, in which photons were predominantly absorbed by quasideuterons.

V. CONCLUSION

The interaction of bremsstrahlung with silver and indium nuclei at an accelerated electron energy of 20 MeV was studied experimentally and theoretically. The yields of photonuclear reactions in ^{107}Ag , ^{113}In , and ^{115}In nuclei were measured, and the yield of the capture reaction of secondary neutrons with the ^{115}In ($9/2^+$) nucleus with the formation of the ^{116m}In (5^+) isomeric state was measured. Monte Carlo simulations were performed using the Geant4 code, and the results were compared with the experimental values. According to the comparison results, the ratio Calc./Exp. was in the range 0.40–2.51. The isomeric ratios of the yields in the reactions $^{107}\text{Ag}(\gamma, n)^{106m,g}\text{Ag}$ and $^{113}\text{In}(\gamma, n)^{112m,g}\text{In}$ were determined, which coincide with literature data. Using the experimental data, the cross sections for the reactions

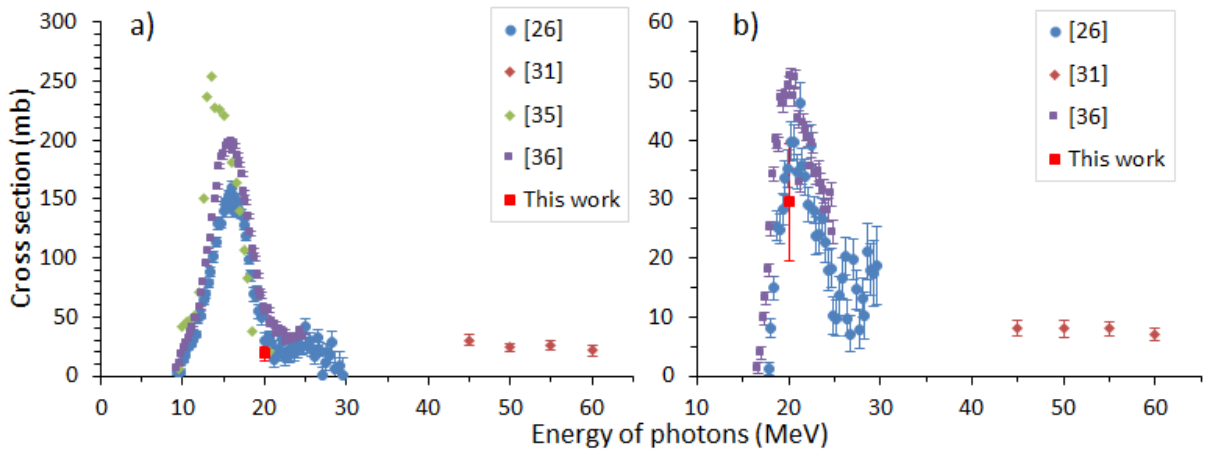


Fig. 3. (color online) Cross sections for the photoneutron reactions $^{107}\text{Ag}(\gamma, n)^{106g}\text{Ag}$ (a) and $^{107}\text{Ag}(\gamma, 2n)^{105}\text{Ag}$ (b).

$^{107}\text{Ag}(\gamma,n)^{106g}\text{Ag}$ and $^{107}\text{Ag}(\gamma,2n)^{105}\text{Ag}$ at an energy of 20 MeV were determined, which also coincide with literature data.

References

- [1] J. R. Huizenga and R. Vandenbosch, *Phys. Rev.* **120**, 13025 (1960)
- [2] R. Vandenbosch and J. R. Huizenga, *Phys. Rev.* **120**, 1313 (1960)
- [3] H. Bartsch, K. Huber, U. Kneissl *et al.*, *Nucl. Phys. A* **256**, 243 (1976)
- [4] Yu. P. Gangrskii, A. P. Tonchev, and N. P. Balabanov, *Phys. Part. Nucl.* **27**, 428 (1996)
- [5] V. M. Mazur, *Phys. Part. Nucl.* **31**, 188 (2000)
- [6] S. A. Karamian, *Phys. Atom. Nuclei* **76**, 1437 (2013)
- [7] S. S. Belyshev, B. S. Ishkhanov, A. A. Kuznetsov *et al.*, *Phys. Atom. Nuclei* **78**, 895 (2015)
- [8] B. S. Ishkhanov, A. A. Kuznetsov, D. E. Lanskoj *et al.*, *Moscow Univ. Phys.* **71**, 215 (2016)
- [9] V. M. Mazur, Z. M. Bigan, and D. M. Symochko, *Phys. Part. Nuclei Lett.* **5**, 374 (2008)
- [10] M. A. Nozdrin, V. V. Kobets, R. V. Timonin *et al.*, *Phys. Part. Nucl. Lett.* **17**, 600 (2020)
- [11] J. Frána, *J. Radioanal. Nucl. Chem.* **257** 3, 583 (2003)
- [12] L. Zavorka, Transmutation of actinides using spallation reactions, PhD thesis, Czech Technical University in Prague, 2015, <http://hp.ujf.cas.cz/~wagner/transmutace/diplomky/zavorka/Lukedis.pdf>
- [13] S. Y. F. Chu, L. P. Ekstrom, R. B. Firestone, The Lund/LBNL Nuclear Data Search, Version 2.0, February 1999, WWW Table of Radioactive Isotopes, <http://nucleardata.nuclear.lu.se/toi/>
- [14] A. J. Koning, D. Rochman, J. Sublet *et al.*, *Nuclear Data Sheets* **155**, 1 (2019)
- [15] J. Allison *et al.*, *Nucl. Instrum. Methods Phys. Res. A* **835**, 186 (2016)
- [16] G. Battistoni, T. Boehlen, F. Cerutti *et al.*, *Ann. Nucl. Energy* **82**, 10 (2015)
- [17] M. E. Rising, J. C. Armstrong, S. R. Bolding *et al.*, MCNP® Code Version 6.3.0 Release Notes, Los Alamos National Laboratory Tech. Rep. LA-UR-22-33103, Rev. 1. Los Alamos, NM, USA. January 2023, https://mcnp.lanl.gov/pdf_files/TechReport_2023_LANL_LA-UR-22-33103Rev.1_RisingArmstrongEtAl.pdf
- [18] Geant4 Collaboration, “Geant4: A simulation toolkit”, Physics Reference Manual, Release 11.1, 2022, <https://geant4-userdoc.web.cern.ch/UsersGuides/PhysicsReferenceManual/fo/PhysicsReferenceManual.pdf>
- [19] V. I. Zhaba, I. I. Haysak, A. M. Parlag *et al.*, *Problems of Atomic Science and Technology* **115**, 155(2018)
- [20] T. D. Thiep, T. T. An, P. V. Cuong *et al.*, *Phys. Part. Nuclei Lett.* **10**, 340(2013)
- [21] A. D. Antonov, N. P. Balabanov, A. G. Belov *et al.*, *Conf. Nucl. Spectroscopy Nucl. Struct.*, Minsk, volume 286, 1991
- [22] N. A. Demekhina, A. S. Danagulyan, and G. S. Karapetyan, *Phys. Atom. Nuclei* **65**, 365 (2002)
- [23] T. D. Thiep, T. T. An, P. V. Cuong *et al.*, *J. Radioanal. Nucl. Chem* **299**, 477 (2014)
- [24] S. R. Palvanov and O. Razhabov, *At Energy* **87**, 533(1999)
- [25] W. Jang, H. Naik, G. Kim *et al.*, *Nucl. Inst. Meth. Phys. Res. B* **537**, 111 (2023)
- [26] M. Tatari, G. Kim, H. Naik *et al.*, *J. Radioanal. Nucl. Chem.* **300**, 269 (2014)
- [27] V. D. Nguyen, D. K. Pham, T. T. Kim *et al.*, *Nucl. Instrum. Meth. B* **342**, 188 (2015)
- [28] M. S. Rahman, K. Kim, T. H. Nguyen *et al.*, *Eur. Phys. J. A* **56**, 235 (2020)
- [29] J. H. Carver, G. E. Coote, and T. R. Sherwood, *Nucl. Phys.* **37**, 449 (1962)
- [30] M. G. Davydov, V. G. Magera, and A. V. Trukhov, *At. Energy* **62**, 277 (1987)
- [31] S. V. Zuyev, V. G. Nedorezov, E. S. Konobeevski *et al.*, *Phys. Atom. Nuclei* **81**, 442 (2018)
- [32] J. H. Khushvaktov, V. I. Stegailov, J. Adam *et al.*, *Phys. Part. Nuclei Lett.* **19**, 347 (2022)
- [33] B. L. Berman, R. L. Bramblett, J. T. Caldwell *et al.*, *Phys. Rev.* **177**, 1745 (1969)
- [34] N. Mutsuro, Y. Ohnuki, and M. Kimura, *J. Phys. Soc. Jpn.* **14**, 1649 (1959).
- [35] A. Lepretre, H. Beil, R. Bergere *et al.*, *Nucl. Phys. A* **219**, 39 (1974).
- [36] M. Zaman, G. Kim, H. Naik *et al.*, *Eur. Phys. J. A* **51**, 5 (2015)